GABA and benzodiazepine agonists and antagonists are probably located in the large N-terminal extracellular domains, which contain a total of 10 potential *N*-glycosylation sites per receptor complex. Such binding site locations are supported by the finding[12] that deglycosylation of the rat $GABA_A$ receptor modifies the binding of benzodiazepine agonists and antagonists. Thus, GABA binding to the β-subunits[5] of the receptor complex would induce a conformational change, exposing some of the positively-charged residues at the channel mouth and possibly shifting the configuration of M1, resulting in chloride ion flux. Allosteric modulation of these conformational changes must be produced by the binding of benzodiazepines or barbiturates. The region linking M3 and M4, which shows no homology between the α- and β-subunits and contains the phosphorylation site, is a potential location for other sites, as yet unknown, mediating intracellular control of channel activity.

The testing of such a model, and the establishment of the mechanisms of channel function and receptor modulation, should be feasible now by means of mutational analysis of the cloned α- and β-subunit cDNAs, coupled with single channel recording in the oocyte expression system.

N.F. holds an EMBO Long-term Fellowship, D.R.B. held a Fogarty Senior International Fellowship and F.A.S. holds a Royal Society University Research Fellowship. We thank Michael Squire (Cambridge) for expert technical help with some of the DNA sequencing, Carole Morita (Genentech) for help with computer graphics and Mary Wynn (Cambridge) for word processing.

Received 26 May; accepted 16 June 1987.

1. Olsen, R. W. & Venter, J. C. (eds) *Benzodiazepine/GABA Receptors and Chloride Channels: Structural and Functional Properties* (Liss, New York, 1986).
2. Turner, A. J. & Whittle, S. R. *Biochem. J.* **209**, 29-41 (1983).
3. Sigel, E., Stephenson, F. A., Mamalaki, C. & Barnard, E. A. *J. biol. Chem.* **258**, 6965-6971 (1983).
4. Sigel, E. & Barnard, E. A. *J. biol. Chem.* **259**, 7219-7223 (1984).
5. Casalotti, S. O., Stephenson, F. A. & Barnard, E. A. *J. biol. Chem.* **261**, 15013-15016 (1986).
6. Mamalaki, C., Stephenson, F. A. & Barnard, E. A. *EMBO J.* **6**, 561-565 (1987).
7. Schoch, P. *et al. Nature* **314**, 168-171 (1985).
8. Huynh, T. V., Young, R. A. & Davis, R. W. in: *DNA Cloning: A Practical Approach*, Vol. 1 (ed. Glover, D. M.) 49-78 (IRL, Oxford, 1985).
9. Von Heijne, G., *Nucleic Acids Res.* **14**, 4683-4690 (1986).
10. Kyte, J. & Doolittle, R. F. *J. molec. Biol.* **157**, 105-132 (1982).
11. Schwartz, R. M. & Dayhoff, M. O. in *Atlas of Protein Sequence and Structure*, Vol. 5, Suppl. 3 (ed. Dayhoff, M. O.) 353-358 (Nat. Biomed. Res. Fdn., Washington DC, 1978).
12. Sweetnam, P. M. & Tallman, J. F. *Molec. Pharmacol.* **29**, 299-306 (1986).
13. Feramisco, J. R., Glass, D. B. & Krebs, E. G. *J. biol. Chem.* **255**, 4240-4245 (1980).
14. Kubo, T. *et al. Eur. J. Biochem.* **149**, 5-13 (1985).
15. Popot, J-L. & Changeux, J-P. *Physiol. Rev.* **64**, 1162-1239 (1984).
16. Criado, M., Sarin, V., Fox, J. L. & Lindstrom, J. *Biochemistry* **25**, 2839-2846 (1986).
17. Kao, P. N. & Karlin, A. *J. biol. Chem.* **261**, 8085-8088 (1986).
18. Goldman, D. *et al. Cell* **48**, 965-973 (1987).
19. Conti-Tronconi, B. M., Hunkapiller, M. W. & Raftery, M. A. *Proc. natn. Acad. Sci. U.S.A.* **81**, 2631-2634 (1984).
20. Hermans-Borgmeyer, I. *et al. EMBO J.* **5**, 1503-1508 (1986).
21. Hucho, F., Oberthür, W. & Lottspeich, F. *FEBS Lett.* **205**, 137-142 (1986).
22. Giraudat, J., Dennis, M., Heidmann, T., Chang, J.-Y. & Chargeux, J.-P. *Proc. natn. Acad. Sci. U.S.A.* **83**, 2719-2723 (1986).
23. Imoto, K. *et al. Nature* **324**, 670-674 (1986).
24. McCarthy, M. P. *et al. A. Rev. Neurosci.* **9**, 383-413 (1986).
25. Grenningloh, G. *et al. Nature* **328**, 215-220 (1987).
26. Ono, J. K. & Salvaterra, P. M. *J. Neurosci.* **1**, 259-270 (1981).
27. Dixon, R. A. F. *et al. Nature* **321**, 75-79 (1986).
28. Kubo, T. *et al. Nature* **323**, 411-416 (1986).
29. Nathans, J. & Hogness, D. S. *Cell* **34**, 807-814 (1983).
30. Sumikawa, K., Houghton, M., Emtage, J. S., Richards, B. M. & Barnard, E. A. *Nature* **292**, 862-864 (1981).
31. Barnard, E. A., Miledi, R. & Sumikawa, K. *Proc. R. Soc. Lond. B* **215**, 241-246 (1982).
32. Smart, T. G., Constanti, A., Bilbe, G., Brown, D. A. & Barnard, E. A. *Neurosci. Lett.* **40**, 55-59 (1983).
33. Houamed, K. M. *et al. Nature* **310**, 318-321 (1984).
34. Melton, D. A. *et al. Nucleic Acids Res.* **12**, 7035-7056 (1984).
35. Dascal, N., Landau, E. M. & Lass, Y. *J. Physiol.* **352**, 551-574 (1984).
36. Study, R. E. & Barker, J. L. *Proc. natn. Acad. Sci. U.S.A.* **78**, 7180-7184 (1981).
37. Bormann, J., Hammill, O. P. & Sakmann, B. *J. Physiol.* **385**, 243-286 (1987).
38. Unwin, P. N. T. *Nature* **323**, 12-13 (1986).
39. Deisenhofer, J., Epp, O., Miki, P., Huber, R. & Michel, H. *Nature* **318**, 618-624 (1985).
40. Rodriguez, H. *J. Chromatog.* **350**, 217-225 (1985).
41. Messing, J., Crea, R. & Seeburg, P. H. *Nucleic Acids Res.* **9**, 309-321 (1981).
42. Hopp, T. P. & Woods, K. R. *Proc. natn. Acad. Sci. U.S.A.* **78**, 3824-3828 (1981).
43. Staden, R. *Nucleic Acids Res.* **10**, 2951-2961 (1982).
44. Barnard, E. A. & Bilbe, G. in *Neurochemistry: A Practical Approach* (eds Turner, A. J. & Bachelard, H.) 243-270 (IRL, Oxford, 1987).
45. Van Renterghem, C. *et al. Molec. Brain Res.* **2**, 21-31 (1987).

LETTERS TO NATURE

Warming of Miranda during chaotic rotation

Robert Marcialis & Richard Greenberg

Lunar and Planetary Laboratory, University of Arizona, Tucson, Arizona 85721, USA

Miranda, a satellite of Uranus, appears in Voyager images to have had an active geological history, seemingly characterized by relaxation of very large-scale topography or the sinking of large blocks of material accreted by the satellite, with associated extrusion, eruption, and flow of the icy material on the body[1]. The low temperature of Miranda (<100 K) would preclude such mobilization of water ice. Hypothetical methane or ammonia constituents have been invoked to circumvent the problem[2]. Here we offer an alternative explanation: topography or anomalous blocks themselves may once have provided the conditions for heating and softening the supporting material, even pure ice, by permitting chaotic rotation of the satellite (J. Wisdom, unpublished lecture). Moreover, this heating mechanism is self-limiting due to rapid damping of the orbital eccentricity. Topography at the presently observed scale (roughly 20 km on this 240-km-radius body) could be preserved.

Chaotic behaviour can occur when resonances are so strong that they overlap[3]. A satellite that rotates synchronously (like the Moon) is in a 1/1 resonance with its orbital motion. This behaviour is stable if the satellite is elongated or has a density asymmetry. Such rotation is maintained by the torque of the planet on the asymmetrical mass distribution. During oscillations about exact synchroneity, the rotation rate can vary to an extent limited by the amount of elongation of the satellite. If the elongation is sufficient, the rate may approach other important resonance rates, such as 3/2 the orbital angular velocity. This case would be an example of an overlapping resonance. Such a non-spherically symmetric, prolate satellite would probably experience chaotic, unpredictable changes in its rotation rate given a wide range of initial conditions.

The criterion for such resonance overlap can be expressed in terms of the principal moments of inertia, $A < B < C$. The quantity $(B-A)/C$ must be greater than ~ 0.1 (ref. 4), which it is for even a slightly prolate body or slightly asymmetric density distribution. For example, an elongation of only about 5% would be sufficient assuming uniform density distribution. Thus, any satellite with moderate asphericity, perhaps due to a high-velocity impact or low-velocity accretion of large components, would be a candidate for chaotic rotation.

Shape is not the only criterion which must be satisfied for chaotic rotation. Additionally, the satellite's orbit must be significantly eccentric in order for spin-orbit resonances other than the 1/1 to be important. If the eccentricity e is too small, a resonance like 3/2 would be too weak to interfere, even if the 1/1 overlaps it. Criteria for adequate e values have not yet been quantified. Hyperion, with $e = 0.1$, almost certainly rotates chaotically[3].

Miranda's geology suggests that the satellite was once non-spherical, whether due to accretion of large blocky constituents[4] or a major impact event. If its orbit were eccentric, it may have rotated chaotically. A non-synchronously rotating satellite has its body worked by tides and is thus heated at the rate

$$dE/dt = 3GM^2(n/a)(k_2/Q)(r/a)^5 \quad (1)$$

where M is the mass of the planet and n, a, k_2, Q and r are

the satellite's mean motion, orbital semi-major axis, Love number, dissipation parameter, and radius, respectively[5]. This formula applies when the rotation rate is of the same order of magnitude as n. For synchronous rotation, tidal heating would be much slower, by a factor of e^2. Chaotic rotation is non-synchronous, so equation (1) applies (J. Wisdom, unpublished lecture).

To evaluate this heating rate, we need an estimate of k_2. For a small rigid satellite like Miranda,

$$k_2 = 3\rho g r/(19\mu) \quad (2)$$

where ρ is the density 1.2 g cm^{-3}, g is the surface gravity 9 cm s^{-2} and μ is the rigidity. Following the estimates of Squyres *et al.*[6] for Enceladus, we adopt values $\mu \sim 4\times10^{10}$ dyn cm^{-2} and $Q \sim 20$, to obtain $k_2 \sim 10^{-3}$ and $dE/dt \sim 6\times10^{18}$ erg s^{-1}. This rate is 10^4 times more than expected due to radiogenic heating alone[7] and ten times more intense per gram than the present tidal heating of Io. Continued heating at such a rate would probably lead to internal softening and relaxation toward a hydrostatic figure, possibly accompanied by surface flows.

This intense heating could not continue for long. The energy must ultimately come out of the satellite's orbit. To conserve angular momentum, the eccentricity must decrease at the rate

$$de/dt = dE/dt/(mn^2a^2e) \quad (3)$$

where m is the satellite's mass. Thus e must plunge to zero in time $t \sim 10^8 e_0^2$ yr, where e_0 is the original value of e. Adopting a reasonable value of $e_0 = 0.1$, we find that $t \sim 10^6$ yr. Because non-zero orbital eccentricity is required to maintain chaotic rotation, the episode of heating terminates in ~1 Myr.

The total heat dissipated in Miranda during that period would have been 2×10^{32} erg. With a heat capacity C_p of $\sim 1.3\times10^7$ erg g^{-1} K^{-1}, the temperature would rise by ~200 K above the surface temperature of 70 K, assuming uniform heating in the body. The temperature rise could not be so great near the surface where conduction removes heat as it is deposited. At the end of the million-year heating period, this cooler boundary layer would have a thickness

$$d \sim (\kappa t)^{1/2} \sim 25 \text{ km} \quad (4)$$

with thermal diffusivity $\kappa \sim 0.15$ cm^2 s^{-1} for ice. The temperature profile would range from 70 K at the surface to the 200 K higher value at 25 km and deeper. Solid-state convection would not occur in this transition layer because at these temperatures the effective viscosity η of ice ($\sim 10^{20}$ g cm^{-1} s^{-1}; see refs 2, 8) is too great and the layer is too thin[9].

The relatively cool upper 25 km has a relaxation time of about 10^6 yr for topography with a horizontal length scale (λ) of 20 km using the above parameters in the following[10]:

$$t = 2\pi\eta/(\rho g\lambda) \quad (5)$$

However, the timescale for substantial cooling in this layer is also about 10^6 yr so the rate of relaxation of 20 km (or smaller) topography would have decreased before much degradation could occur.

For larger structure (greater λ), such as the global non-hydrostatic figure that permitted chaotic rotation, the relaxation timescale is shortened by two factors: first, the inverse λ dependence in equation (5) and second, an additional factor that accounts for the much-reduced viscosity[2,8] at the higher temperature below 25 km. This second factor is unity for $\lambda < d$, but is 0.5 for $\lambda = 100$ km and 0.1 for λ near 240 km, the radius of the satellite[10]. Thus global scale topography would have relaxed away before the satellite cooled down from its chaotic rotation heating. Numerical integration of the heat flow equation shows that all vestiges of the implanted heat will be dissipated within 100 Myr.

This explanation of the heat source for geological activity, the relaxation of global structure, and retention of significant local topography does not require any hypothetical constituents added to the water ice. In contrast, Stevenson and Lunine[2] hypothesize an intergranular cryogenic fluid such as methane to obtain lower viscosities so that deformation can occur at low temperatures. Similarly, Squyres *et al.*[6] had to assume a eutectic mix of water and ammonia in order to bring about even marginal melting of Enceladus.

Our calculation of the total heat dissipated during chaotic rotation, and of the corresponding internal temperature rise is independent of the 30% uncertainty in Miranda's mass[1] and of the much greater uncertainty in the value of k_2/Q. We have adopted the same minimal value for Q as Squyres *et al.*[6]. A larger value of Q would slow the heating rate, but lengthen the chaotic era, preserving the total energy deposited. The depth of the conduction layer increases, but only as $Q^{1/2}$. Also, any effect of a larger Q would be counteracted by an increase in the value of k_2 that would have accompanied the warming and softening of the interior.

The total energy dissipated is very sensitive to the initial eccentricity e_0, because the duration of the chaotic rotation is proportional to e_0^2. For our calculations, we have assumed a plausible value $e_0 \sim 0.1$ and demonstrated that the appropriate amount of heating could take place. Such a value could have been primordial. It is comparable to the present orbital inclination in radians[1]. Perhaps e_0 was generated by some past orbital resonance, such as a resonance with Ariel that may have been traversed during tidal evolution of the satellites' orbits[11]. If e_0 were a few times smaller, the heating of Miranda would have been greatly reduced. In that case, the effects we describe might still have occurred given a somewhat smaller heat capacity, or the presence of impurities such as methane or ammonia which would permit equivalent softening with less heat.

If the heating process described here were active before the cratering and basin-forming bombardment of Miranda's surface, all geological evidence would have been destroyed. Certainly any geological expression of accretional heating (which by definition occurred early and which was at most only marginally adequate to have significant effect) must have been erased. On the other hand, it is plausible that chaotic rotation and heating took place later on. The last basin-forming events appear to have occurred after formation of the cratered terrain[12]. If these large impacts gave the modest asymmetry needed for chaotic rotation, our mechanism could have heated Miranda after most craters were in place. These ideas will be tested as a complete geological chronology emerges.

It is possible that some or all of the other icy satellites of comparable size to Miranda experienced similar chaotic rotation if their figures were originally comparably irregular[3]. Repeating the above calculation for the inner satellites of Saturn and for the other satellites of Uranus shows that they could have been heated comparably to Miranda. With the same assumed initial eccentricity, we find they generally would have received several times more heat per volume than Miranda. They would have been overheated from the point of view of retaining even local topographic structure. Irregularities in global shape surely would have been eliminated and the interiors differentiated. Melt flows on the surface might have been created, and then possibly erased, depending on the impact chronology in each case. For those satellites whose eccentricities were always small, tidal heating would have been negligible even during chaotic rotation. Today, only Hyperion remains in chaotic rotation. Its resonance with Titan maintains the eccentricity, but at its great distance from Saturn it does not heat up very much. According to our model, Miranda's eccentricity damped away allowing just enough heating for global relaxation and geological activity, yet allowing local topography to be retained.

We thank J. A. Burns, S. Croft, J. Lunine, H. J. Melosh, S. J. Peale and J. Wisdom for helpful discussions and review of this manuscript. Croft provided the estimates of thermal diffusivity and heat capacity used in our calculations.

Received 12 January; accepted 24 April 1987.

1. Stone, E. C. & Miner, E. D. *Science* **233**, 39-43 (1986).
2. Stevenson, D. J. & Lunine, J. I. *Nature* **323**, 46-48 (1986).
3. Wisdom, J., Peale, S. J. & Mignard, F. *Icarus* **58**, 137-152 (1984).
4. Kerr, R. A. *Science* **235**, 31 (1987).
5. Hubbard, W. B. *Planetary Interiors* 96-102 (Van Nostrand Reinhold, New York, 1984).
6. Squyres, S. W., Reynolds, R. T., Cassen, P. M. & Peale, S. J. *Icarus* **53**, 319-331 (1983).
7. Schubert, G., Spohn, T. & Reynolds, R. T. in *Satellites* (eds Burns, J. A. & Matthews, M. S.) 224-292 (University of Arizona Press, Tucson, 1986).
8. Poirer, J. P. *Nature* **299**, 683-688 (1982).
9. Cassen, P. M. & Reynolds, R. T. *Geophys. Res. Lett.* **6**, 121-124 (1979).
10. Melosh, H. J. *Impact Cratering: A Geological Process* (Oxford University Press, in the press).
11. Peale, S. J. *Bull. Am. astr. Soc.* **18**, 785 (1986).
12. Croft, S. K. *Lunar planet. Sci.* **XVIII** 207-208 (1987).

Experiments on laser guide stars at Mauna Kea Observatory for adaptive imaging in astronomy

Laird A. Thompson* & Chester S. Gardner†

* Institute of Astronomy, University of Hawaii at Manoa, 2680 Woodlawn Drive, Honolulu, Hawaii 96822, USA
† Department of Electrical and Computer Engineering, University of Illinois at Urbana-Champaign, 1406 West Green Street, Urbana, Illinois 61801, USA

Atmospheric turbulence severely limits the resolution of ground-based astronomical telescopes. Under good seeing conditions at the best observatory sites, resolution at visible wavelengths is typically limited to about 1 arc s. During the past 15 years, adaptive optical systems with electrically deformable mirrors have been developed to compensate for turbulence[1,2]. Unfortunately, these systems require bright reference sources adjacent to the object of interest and can only be used to observe the brightest stars. Foy and Labeyrie[3] were the first to suggest that lasers could be used to create artificial guide stars that might be suitable in controlling an adaptive imaging system. We have recently extended this concept in two ways. First, we have identified the key engineering parameters that optimize the performance of a laser-guided imaging system. Second, on the nights of 21 and 22 January 1987, we conducted experiments at the Mauna Kea Observatory on the island of Hawaii to test the feasibility of using a laser to generate an artificial guide star in the mesospheric sodium layer. Here we describe both the engineering calculations and the results of our first experiments.

The angular resolution of a ground-based telescope is $1.22\lambda/r_0$, where λ is the optical wavelength and r_0 is the diameter of the turbulence seeing cell. At the best observatory sites, under good seeing conditions, $r_0 = 10$–20 cm, and at a few outstanding sites, such as Mauna Kea, r_0 can exceed 40 cm on rare occasions. If the diameter of the telescope is less than r_0, a diffraction-limited image will be focused onto the image plane[4]. However, tilt caused by turbulence makes the image dance about so that long-term exposures are blurred. If the object is bright enough, a dynamic tip-tilt mirror can be used to stabilize the image[5].

When the telescope diameter (D) is larger than r_0, each seeing cell within the pupil generates a subimage of angular radius, $1.22\lambda/r_0$, that dances in the image plane independently of the subimages from every other seeing cell. Modern adaptive telescopes use a wavefront sensor consisting of a lenslet array followed by a quadrant detector array to measure the centroid positions of each seeing cell subimage. This information is then used to control the deformable mirror[1,2]. A quadrant detector can determine a subimage centroid with an angular accuracy given approximately by

$$\frac{0.61\lambda/r_0}{\sqrt{N}} \tag{1}$$

where N is the subimage photon count during the measurement integration period. The integration time is limited to the turbulence coherence time which is typically ~10 ms. To achieve diffraction-limited performance, each subimage centroid must be determined with an accuracy sufficient to reduce the wavefront tilt to ~1/3 of the residual wavefront distortion remaining in a perfectly tilt-corrected seeing cell (namely, $\sim\lambda/17$).

$$\frac{0.61\lambda/r_0}{\sqrt{N}} \approx \frac{1}{3}\frac{4}{r_0}\frac{\lambda}{17} \approx 0.8\frac{\lambda}{r_0} \tag{2}$$

Thus, the required photon count at each quadrant detector is $N \approx 60$. To reach the diffraction limit of any ground-based telescope, the required signal levels are very large. Because very few interesting astronomical objects are sufficiently bright or have a suitable guide star located near them, adaptive imaging systems have found only limited use in astronomy.

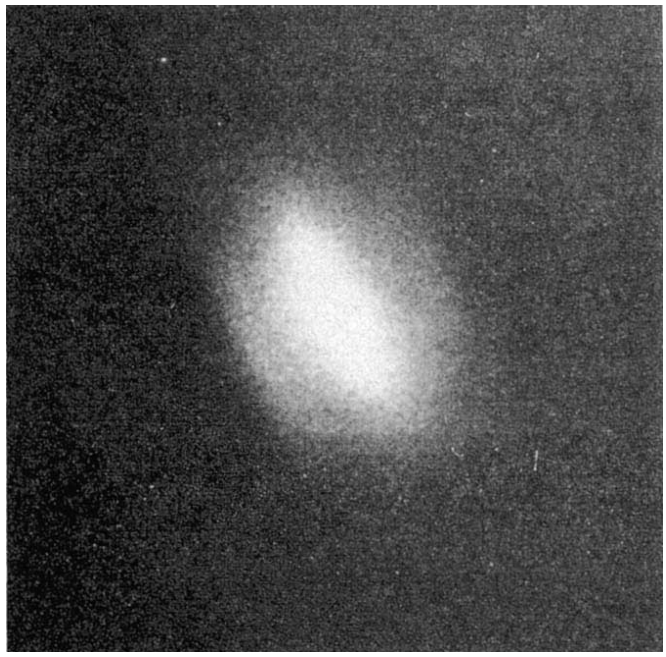

Fig. 1 Image of the laser guide spot obtained on 21 January 1987; exposure time was 8 min starting at 13:43 UT. The image is asymmetric because of the laser beam divergence, imaging geometry and the finite thickness of the sodium layer. The laser beam enters the layer from the top left and leaves towards the lower right. The telescope was fixed near zenith so that background stars drifted through the field of view during the exposure. Two such trails cut horizontally across the image. North is to the top and east to the left.

Laser-guide stars can be generated in the upper atmosphere by either Rayleigh scattering by air molecules in the stratosphere or resonant scattering by alkali metals in the mesosphere. By calculating the laser power requirements for each technique, we find that resonant scattering by sodium atoms is the preferred approach. The chemistry and dynamics of the sodium layer have been studied extensively since the late 1960s with lidar techniques[6,7]. Meteoric ablation is generally regarded as the dominant source of all mesospheric alkali metals including sodium. The sodium layer is typically confined to the region between 80 and 110 km with a peak near the mesopause at 90 km, where the density ranges from $\sim 10^3$–10^4 cm^{-3}. The sodium column abundance at mid-latitidues in the Northern Hemisphere varies from a summer minimum of $\sim 2\times10^9$ cm^{-2} to a winter maximum of $\sim 10^{10}$ cm^{-2} in December and January[6]. The seaosonal and geographical variations in sodium abundance are now believed to be related to changes in the mesopause temperature that affect the reaction rates of the main chemical loss processes for sodium. For adaptive imaging, sodium abundance is an important parameter because the brightness of a guide